Received: 18 December 2020 | Revised: 15 February 2021 | Accepted: 3 March 2021

DOI: 10.1049/hve2.12096

High Voltage

ORIGINAL RESEARCH PAPER

Hybrid piezo/triboelectric nanogenerator for stray magnetic energy harvesting and self-powered sensing applications

Aijun Yang | **Chaoyu Wang** | **Jing Ma** | **Chengyu Fan** | **Pinlei Lv** | **Yuchen Bai** | **Yiming Rong** | **Xiaohua Wang** | **Huan Yuan** | **Mingzhe Rong**

State Key Laboratory of Electrical Insulation and Power Equipment, Xi'an Jiaotong University, Xi'an, China

Correspondence

Xiaohua Wang, State Key Laboratory of Electrical Insulation and Power Equipment, Xi'an Jiaotong University, Xi'an, China.
Email: xhw@mail.xjtu.edu.cn

Associate Editor: Xingyi Huang

Funding information

The State Grid Corporation of China, Grant/Award Number: 52094020006Z

Abstract

Stray magnetic fields with a fixed frequency of 50/60 Hz are ubiquitous in buildings, factories, and power system equipment. Researchers are increasingly focusing on harvesting electrical energy from stray magnetic fields to provide sustainable energy for the Internet of Things (IoT) devices. Magneto-mechano-electric energy conversion is the most efficient way to convert low-frequency stray magnetic fields into electricity. In this study, we proposed a hybrid piezo/triboelectric nanogenerator (HP/TENG) on the basis of a cantilever beam to use stray magnetic fields from the surrounding environment. The hybrid nanogenerator provided high output voltage/current and power of ~176 V/375 μA and 4.7 mW (matched impedance of 20 kΩ) in a magnetic field environment of 4 Oe. The device provided a stable 3.6 V direct current output by incorporating energy management circuitry to sustainably drive power to commercial wireless temperature/humidity sensors. The HP/TENG has a significant application potential in IoT, which can use stray magnetic energy and a power wireless sensor system.

1 | INTRODUCTION

Energy harvesting devices have been extensively researched as a response to the global energy crisis. With the development of the Internet of Things (IoT), numerous portable and distributed electronic devices, such as sensors and wireless transmission systems are required in high-voltage transmission or insulation monitoring [1–11]. High-capacity batteries are currently powering the sensors. When sensors are deployed on a large scale, battery replacement and maintenance are challenging. Simply using batteries to power a wireless sensor network is unfeasible. Thus, the best approach is to develop various self-powered IoT devices that continuously collect energy from the environment [12–14].

Energy harvesting technology allows generating electrical power from the surrounding environment, such as mechanical vibrations [15], heat [16], sunlight, tides/waves [17] and stray magnetic fields [18]. Of these, the magnetic field is a promising and reliable source of energy because of the stray magnetic field caused by power cables in most environments, such as buildings, power equipment and factories.

Magneto-mechano-electric (MME) generators have gained extensive attention because of their ability to generate high power density under low-frequency magnetic field conditions to supply power to IoT devices [19, 20]. MME generators comprise a piezoelectric cantilever beam with permanent magnet tip mass and magnetostriction materials. The magnetic field energy is converted into mechanical vibration through the magnetostriction effect and the force of the permanent magnet in the magnetic field. The electric field is generated through the piezoelectric effect because of the mechanical motion.

Xing et al. [21] first proposed an energy harvesting system on the basis of permanent magnets and piezoelectric cantilever beams, which showed excellent efficiency in magnetic energy harvesting at low frequencies. Liu et al. [22] obtained a maximum power density of 11.73 $\mu W/cm^3$ at 100 μT and 100 Hz resonant excitation by designing dual piezoelectric crystals and tip magnets for low-frequency magnetic energy harvesting. Kang et al. [23] proposed an MME harvester incorporating magnetoelectric composites that produced a high output power of up to 9.8 mW at 1 mT alternate current (AC) magnetic field. Lee et al. [24] demonstrated a novel magnetoelectric effect coupled MME

generator that generated milliwatt power below the 300 μT stray fields. The device could also light up hundreds of light-emitting diode arrays with average output power and operate a digital clock without charging capacitors at low magnetic fields (≤50 μT). By optimizing the direction of magnetization by vertically adjusting the flux direction of the power cord and magnetic direction of the tip magnet, Cho et al. [25] obtained a high electrical power of 39.2 mW (planar–vertical) at 5 kΩ for the magnetic piezoelectric energy harvester. Lu et al. [18] reported a Pb(Zr, Ti)O_3 (PZT)/Ni single piezoelectric wafer cantilever with a permanent magnet (NdFeB) tip, coupled by the magnetostriction of the Ni beam to the magnetic torque of the NdFeB magnets, with a maximum power density of 270 μW/cm^3. The device could power a commercial wireless temperature/humidity sensor.

The hybrid use of multiple types of energy harvesters allows for the simultaneous harvesting of power from several types of energy sources, providing an effective way to enhance the output power. According to triboelectrification and electrostatic induction, the triboelectric nanogenerator (TENG) is widely used to derive electrical energy from mechanical and vibrational energy because of low cost, high throughput and lightweight solutions. Huang et al. [26] demonstrated the magneto-mechano-triboelectric nanogenerator (MMTENG) by fabricating composites with polydimethylsiloxane (PDMS) and Fe–Co–Ni powder to exert the role of triboelectrification collection and magnetic field responsive vibrating materials. The device can generate maximum voltages and currents of 275 V/9 μA under 10 Hz and 5 KOe AC magnetic fields, respectively. Lim [27] constructed a cantilevered MMTEG with NdFeB magnets as tip mass, perfluoroalkoxy and aluminium (Al) foil as triboelectric materials, with open-circuit voltage up to 708 V and short-circuit current up to 277 μA at 7 Oe AC magnetic field. Several hybrid energy harvesters have been utilized to harvest mechanical, wind, vibrational and blue energy [28–36]. However, the combination of MME and MMTENG has not been specifically reported for electromagnetic energy harvesting. Because the MME generator collects mechanical vibrations under stray magnetic fields, the electrodes of the TENG and active materials can be attached to the piezoelectric device to convert mechanical energy into electrical energy and further increase the total power output.

We propose a hybrid piezo/triboelectric nanogenerator (HP/TENG) on the basis of a cantilever beam to use stray magnetic fields from the surrounding environment. The hybrid nanogenerator was based on a titanium (Ti) sheet as the cantilever beam, with PDMS and Al foil as triboelectric materials and PZT as a piezoelectric material. Finite element COMSOL simulation was used to design the device structure with the best resonance modes improving the output performance. Under the synergistic effect of triboelectric initiation and piezoelectric polarization, the HP/TENG presented high open-circuit voltage (176 V), short-circuit current (375 μA) and maximum output power of ~4.7 mW under an AC magnetic field of 4 Oe induced by the Helmholtz coil. When both mechanisms worked, the HP/TENG produced a total power approximately 2.08 times higher than the piezoelectric nanogenerator (PENG) and approximately 2.14 times higher than the TENG at optimal matching impedance. Furthermore, the device was used with energy management circuitry to sustainably operate commercial wireless temperature and humidity sensors, revealing potential applications for self-powered wireless sensing systems.

2 | DESIGN OF THE HP/TENG

Figure 1a shows the HP/TENG on the basis of a cantilever beam structure, achieving efficient energy conversion from the surrounding stray magnetic field. The device comprises the PENG with a single circular PZT-5H type structure at the top of the cantilever beam and the contact-separated TENG with a PDMS/Al electrode at the bottom. The Al foil (thickness 40 μm) was attached to the Ti substrate (thickness 300 μm) underneath. The Ti sheet and the Al electrode were insulated from each other by a tape (thickness 10 μm). The PDMS with back-sputtered copper electrodes was attached to the acrylic plate by the foam adhesive. The permanent magnet NdFeB was attached to the beam end as a tip mass block and played two roles: (i) to make the cantilever beam vibrate up and down reciprocally under an AC magnetic field to drive the mechanical motion by magnetic torque and (ii) to adjust the resonant frequency of the piezo/triboelectric hybrid generator to match that of the power supply (50 Hz). The resonant frequency of the acquisition device can be regulated by adjusting the number or position of the magnets. For a cantilever with a given tip mass, the distribution of the resonant frequency (ω_0) of the cantilever beam can be obtained using Equation (1) [31].

$$\omega_0 = \sqrt{\frac{k_{eq}}{m_{eq}}} = \sqrt{\frac{3EI/L^3}{(33/140)mL + M_t}} \tag{1}$$

where k_{eq}, m_{eq}, EI, L, m and M_t are equivalent spring constants of the cantilever, equivalent mass, flexural stiffness of the beam, length of the beam, mass per unit length and tip mass, respectively.

The relationship suggests that flexural stiffness, beam length and the weight of the tip mass are influential factors in fixing the resonant frequency. The magneto-mechanical torque (τ) of a permanent magnet under an external magnetic field can be expressed as Equation (2) [32].

$$\tau = (\boldsymbol{M} \times \boldsymbol{B}) \cdot \boldsymbol{V} \tag{2}$$

where $\boldsymbol{M}$, $\boldsymbol{B}$ and $\boldsymbol{V}$ are the magnetization intensity, the external magnetic field and volume of the permanent magnet, respectively. Because the resonance frequency is fixed at 50 Hz, we modified the HP/TENG structure, of which the dimensions of the Ti beam are 100 mm (length) × 20 mm (width) × 0.3 mm (thickness), including a 10 mm clamping area at one end. The piezoelectric element was a PZT-5H ceramic plate (polarized along the thickness) with a diametre of 25 mm and a thickness of 0.3 mm. Commercial rectangular NdFeB magnets (type N52) were attached to the free end of the Ti beam. The piezoelectric elements were adhered to the Ti beam using glue and cured for 24 h at room temperature.

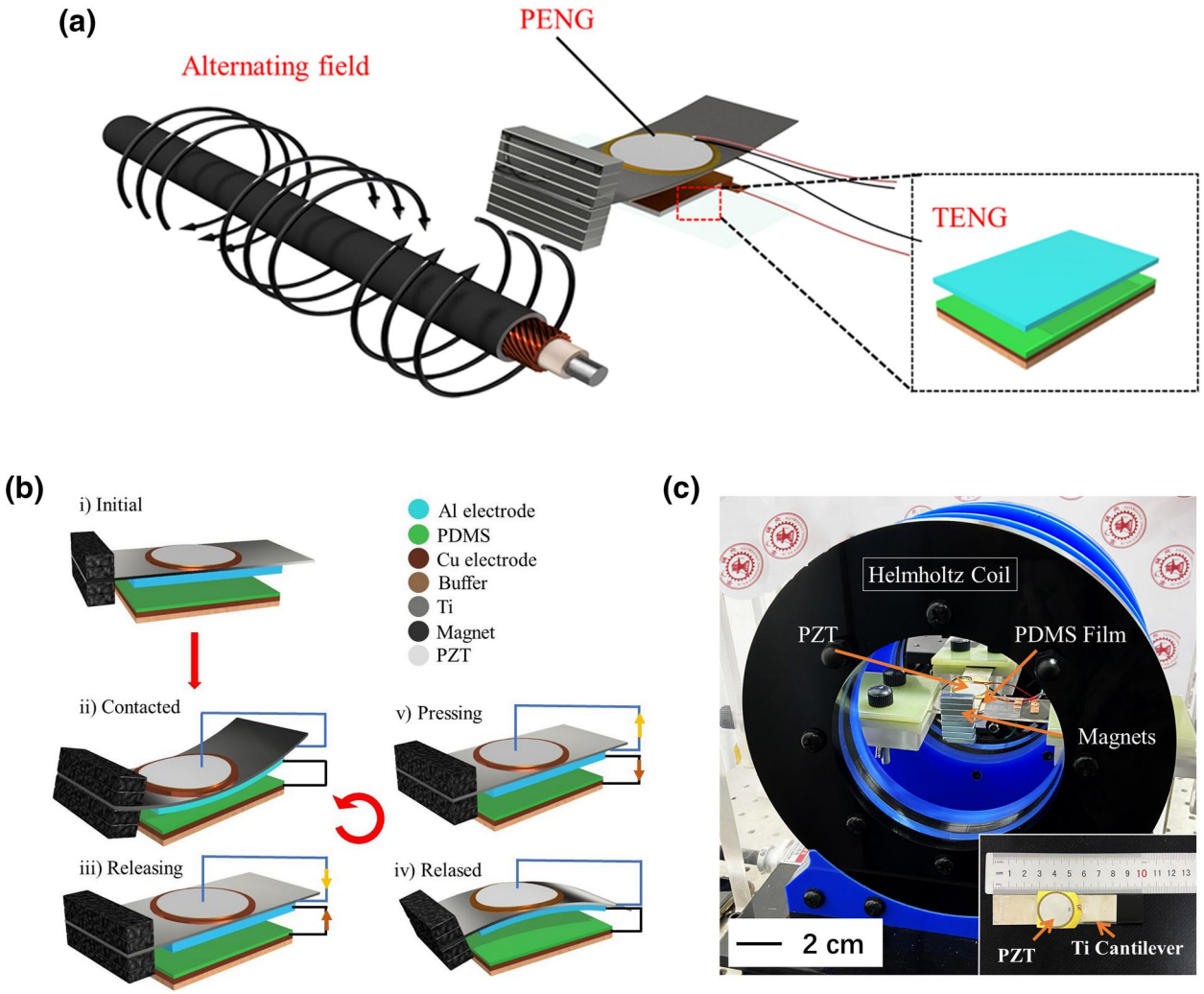

FIGURE 1 Experimental principle: (a) schematic of hybrid piezo/triboelectric nanogenerator under an AC magnetic field, (b) illustrations of the working mechanism of the HP/TENG in an AC magnetic field and (c) photograph of the HP/TENG system

The HP/TENG uses the normal piezoelectric effect, the triboelectric effect, electrostatic induction and reciprocating motion of the cantilever beam under the AC magnetic field. Figure 1b illustrates the working mechanism of the HP/TENG. Initially, there is neither piezoelectric potential nor triboelectric potential, and no charge transfer occurs before the vibration of the cantilever beam and contact of two triboelectric layers (Figure 1b(i)). Under the action of the external magnetic field, the structural movement of the cantilever beam brings the Al foil and PDMS film into contact, where negative triboelectric charges are generated on the PDMS's upper surface, and the Al foil generates positive triboelectric charges. Because of the bending and deformation of the cantilever beam, the piezoelectric functional layer PZT is subjected to compressive stress, which results in the generation of positive and negative electrons on the Ag electrode on the PZT surface as well as on the Ti sheet (Figure 1b(ii)). The positive and negative triboelectric charges remain on the surfaces of the PDMS and Al when these two contact surfaces start to separate, inducing opposite charges on the Cu electrode of the PDMS film. During the releasing process, the piezoelectric part returns to its original state and is subjected to stretching gravitational forces. The output electrons flowing in the circuit between the Ag electrode and the Ti sheet are driven by the potential difference (Figure 1b(iii)). Figure 1b(iv) shows that the potential difference between the triboelectric parts and the piezoelectric potential to meet the condition that conservation of charge generates the electron flow until a fully released state is reached. Subsequently, the downward movement of the cantilever decreases the gap distance between the two triboelectric layers, and the change in potential difference causes electrons to flow from the top Al to the bottom Cu electrode. Meanwhile, the piezoelectric functional layer is deformed by the opposite stress, causing electrons to flow in the opposite direction (Figure 1b(v)). The Helmholtz coil (Figure 1c) can generate a uniform AC magnetic field around the HP/TENG by controlling the input AC (Figure S1).

3 | THE OUTPUT PERFORMANCE OF THE HP/TENG

We investigated the output performance of HP/TENG in Helmholtz coils. The entire area of the cantilever structure was $100 \times 20\ mm^2$, and the effective area of the triboelectric PDMS

film was 30 × 20 mm^2 (Figure S2). The resonant frequency of the HP/TENG is 50 Hz attained by placing eight magnet blocks (total weight 32 g) at the end of the cantilever.

We measured the output voltage of PENG and TENG in response to different magnetic fields from 2 Oe to 8 Oe (Figure S3). The output voltage increased with an increasing magnetic field, and the increase in voltage from 6 Oe tended to be slow. With an AC magnetic field of 4 Oe and 50 Hz, the maximum rectified output voltage and current of the TENG were 168 V and 15 μA (Figure 2d and e), and the maximum rectified voltage and current of the PENG were approximately 15 V and 350 μA, respectively (Figure 2a and b). The PENG showed high output current and low output voltage, appropriately complementing the output performance of the TENG. The output characteristics of the HP/TENG were studied by connecting two rectifier circuits in parallel after connecting two independent full-wave diode bridges to rectify PENG and TENG, respectively (Figure S4). The maximum output voltage and current of the HP/TENG were 176 V and 375 μA (Figure 2g and h). The HP/TENG output voltage variation and peak power were obtained by connecting the resistor box in series with the rectifier circuit. The voltage first increased and then smoothed with the increasing resistance, and the power increased first with the load change and then decreased. The peak output power of TENG was 2.2 mW at a matching impedance of 6 MΩ, and the peak output power of PENG was 2.25 mW at a matching impedance of 20 kΩ (Figure 2c and f). The output voltage of the hybrid nanogenerator was slightly higher than that of TENG, and the output current was similar to that of PENG. The hybrid nanogenerator inherited the advantages of PENG and TENG (i.e. high output voltage and high current), and the maximum output power was ~4.7 mW with matching impedance of ~20 kΩ (Figure 3a). When both mechanisms worked, the HP/TENG produced a total power of approximately 2.08 times higher than that of the PENG and approximately 2.14 times higher than that of the TENG at the optimal matching impedance. In order to investigate the effect of frequency on the output performance of the hybrid nanogenerator, it was experimentally found that the resonant frequency of the PENG and TENG was 50 Hz, which was consistent with the sinusoidal excitation

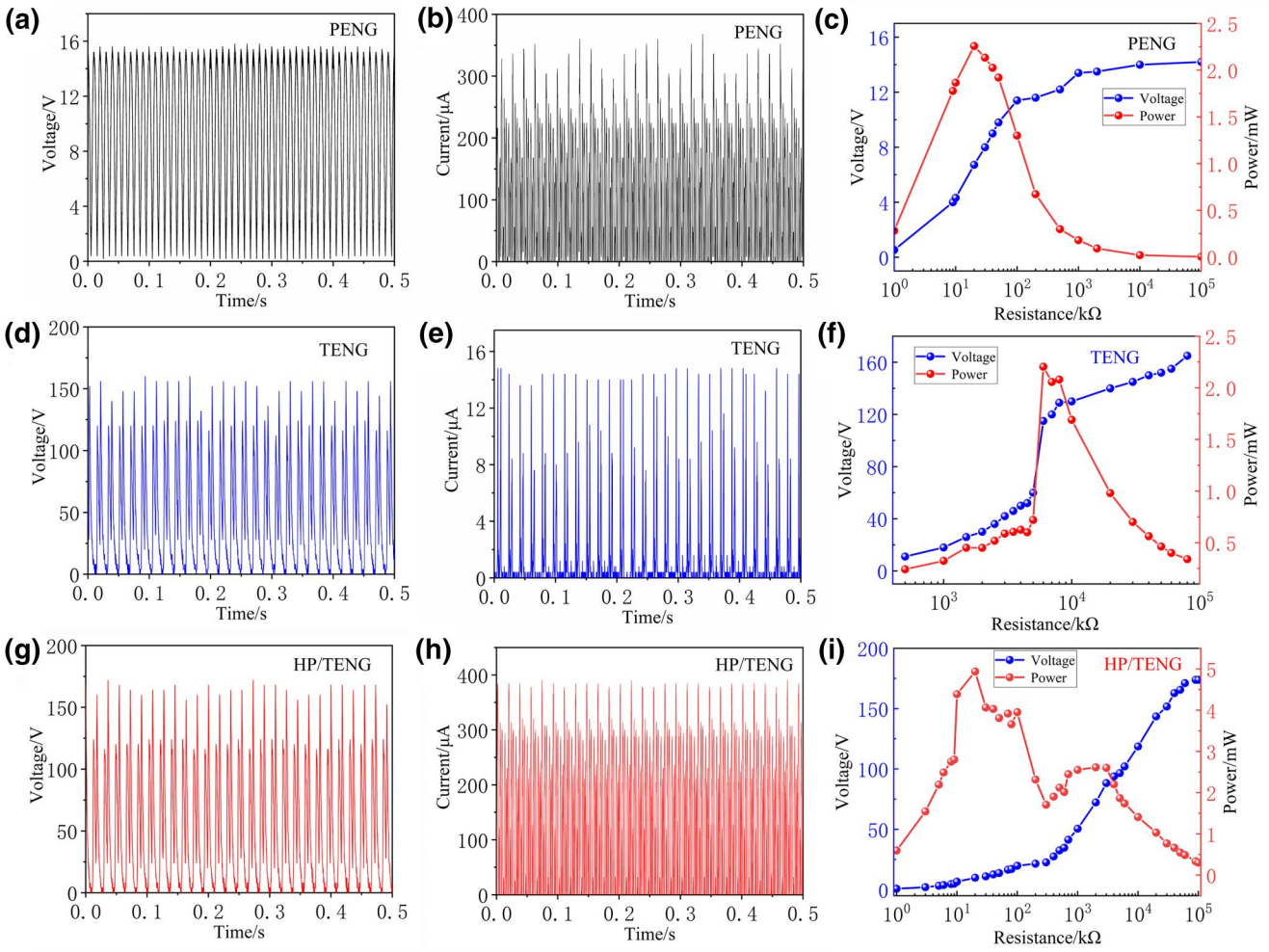

FIGURE 2 Output characteristics of rectified PENG, TENG and HP/TENG at a magnetic field strength of *4* Oe: (a)(b) the rectifier open-circuit voltage and short-circuit current of PENG, (c) the output voltage and power of PENG vary with the external load resistance, (d)(e) the rectifier open-circuit voltage and short-circuit current of TENG, (f) the output voltage and power of TENG vary with the external load resistance, (g)(h) the rectifier open-circuit voltage and short-circuit current of HP/TENG and (i) the output voltage and power of HP/TENG vary with the external load resistance

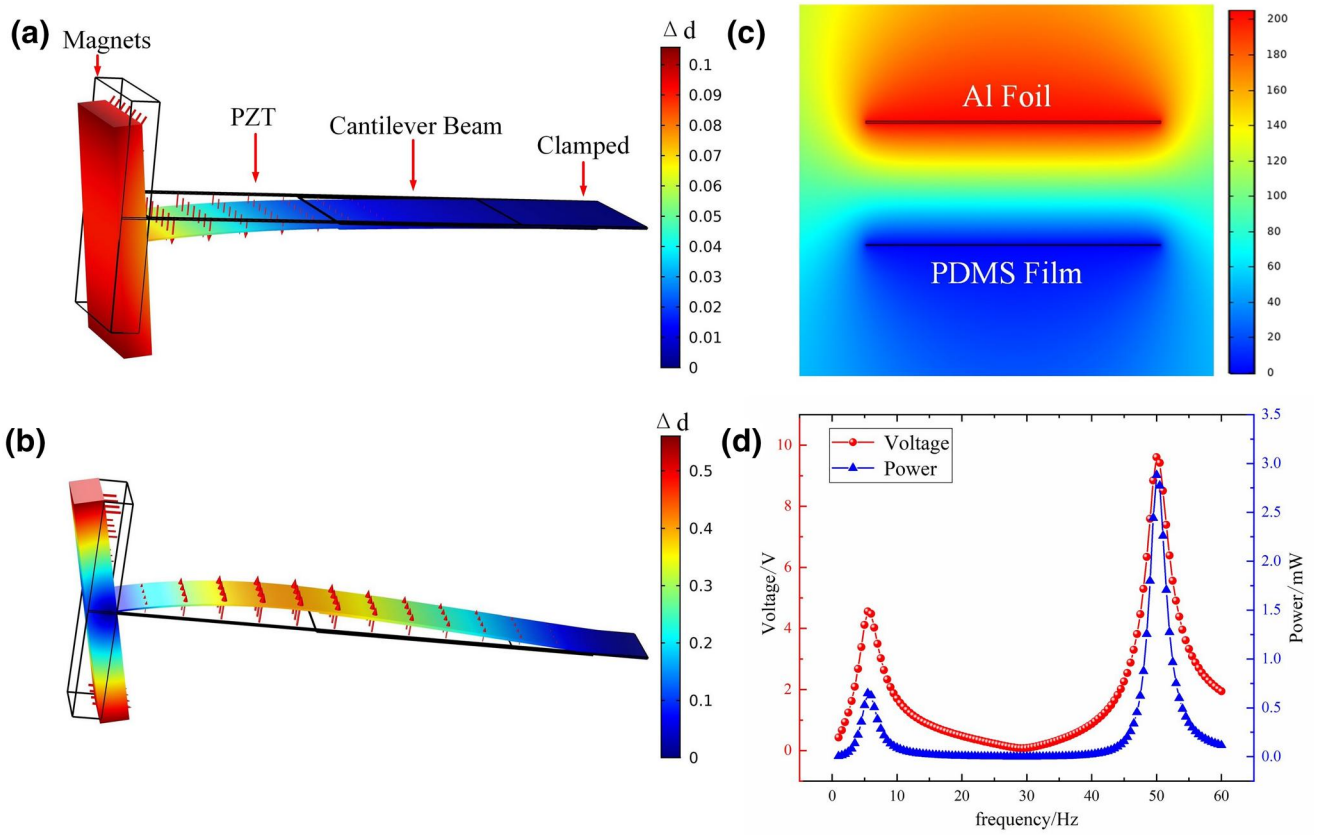

FIGURE 3 Experimental simulation: (a) simulated motion shapes of MMTEG cantilever structures in the second bending resonance mode, (b) simulated motion shapes of MMTEG cantilever structures in the first bending resonance mode, (c) calculated electrostatic potential with top Al part and flat PDMS surface and (d) the simulation of output voltage and power

TABLE 1 Setting parameters of the multiphysics simulation model for the present study

Parameters	Value	Unit
Residual flux density of the magnet	1.2	T
The size of the magnet	20 × 20 × 5	mm^3
The size of PZT	50 × 20 × 2	mm^3
The size of the titanium sheet	100 × 20 × 3	mm^3
The size of the Al foil	70 × 20 × 0.03	mm^3
External magnetic field strength	5	Oe
AC frequency	50	Hz

frequency provided by the Helmholtz coil. Therefore, this study improved the output performance when the nanogenerator operated at 50 Hz under resonant conditions, as shown in Figure S6.

4 | WORKING MECHANISMS OF THE HP/TENG

We elucidated the working mechanism of the cantilevered HP/TENG by conducting theoretical simulations. Unlike conventional energy harvesters, the hybrid nanogenerator was not driven by direct vibration from the outside world but by electromagnetic forces generated by the external magnetic field and the magnetic field of permanent magnets. Therefore, we predicted the power generation performance of the hybrid MME generator by constructing a multiphysics field simulation model of the hybrid nanogenerator by introducing electrostatics, solid mechanics and electromagnetism. Finite element COMSOL software simulation analysed the triboelectric potential generated by the mechanical resonance mode and the piezoelectric potential. Table 1 shows the input parameters for the multiphysics field simulation model used in this study.

Figure 3a and b shows the simulated operating shape of the hybrid nanogenerator cantilever structure in the first and second bending resonance modes. Δd is the displacement of the structure. Based on the analysis in [13], we found that the middle region of the triboelectric cantilever had the largest displacement of vibratory motion in the second harmonic bending mode and provided a larger effective triboelectric starting area during the harvesting operation, significantly improving the triboelectric and piezoelectric potential output. Thus, we adopted the second bending resonance mode for the HP/TENG. Based on the Gaussian theorem, the voltage of TENG (V_{OC}) is described by Equation (3) [28].

$$V_{oc} = -\frac{Q}{S\varepsilon_0}\left(\frac{d}{\varepsilon_1} + x\right) + \frac{\sigma x}{\varepsilon_0} \quad (3)$$

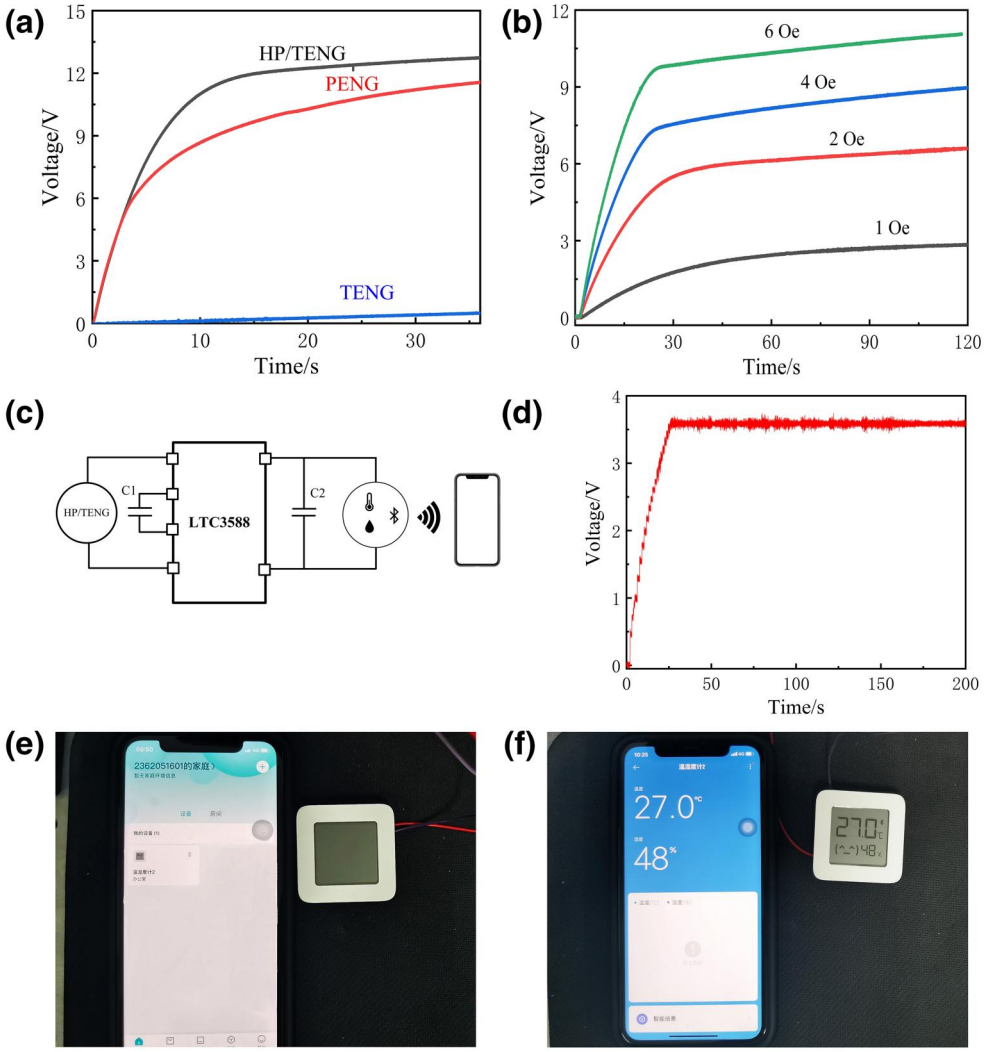

FIGURE 4 Demonstration of the HP/TENG to power wireless sensors: (a) 47 μF capacitor charged by TENG, PENG and HP/TENG in a 4 Oe magnetic field, (b) the charging voltage of 220 μF/25 V storage capacitor under different magnetic field conditions, (c) circuit diagram for a complete DC power supply with a constant output voltage of 3.6 V, (d) constant output voltage of the measured DC power supply, (e) status with temperature and humidity sensor off and (f) the self-powered system drove the temperature and humidity sensor

where Q is the amount of charge transferred between the two electrodes by electrostatic induction, x is the distance between the two friction layers, d, σ, S, ε_1 and ε_0 are the thickness of the friction layers, the surface charge density, electrode area, dielectric PDMS constant and vacuum dielectric constant, respectively. Equation (3) shows that the voltage of the TENG predominantly depended on the amount of transferred charge and the surface charge density. According to this formula, the maximum triboelectric charge density σ of 0.56 μC/m^2 was obtained on the flat PDMS surface in the open-circuit state by applying a maximum V_{OC} of 190 V (Figure 3c) and a maximum distance x of 3 mm. We used the 2-D magnetic field module of COMSOL software to calculate the magnetic force of a single cross-section of a permanent magnet in the AC magnetic field and multiplied it by the thickness to find the magnetic force of the whole permanent magnet. Finally, we applied the equivalent magnetic force to the surface of the permanent magnet. The magnitude of the magnetic force under the action of the AC magnetic field can be calculated by applying the Maxwell surface stress tensor to the surface of the permanent magnet, where the expression for the Maxwell surface stress tensor is $\boldsymbol{T_m}$.

$$\boldsymbol{T_m} = \boldsymbol{BH} - \boldsymbol{P_{em}}\boldsymbol{I} \tag{4}$$

where $\boldsymbol{B}$, $\boldsymbol{H}$, $\boldsymbol{P_{em}}$ and $\boldsymbol{I}$ are the magnetic susceptibility tensor, magnetic field tensor, the magnetic pressure and unit matrix, respectively. Using the piezoelectric principle equation, the relationship between strain and generation is calculated. The conservation of charge equation for piezoelectric materials can be given by:

$$\nabla \cdot \boldsymbol{D} = \rho_v \tag{5}$$

$$\boldsymbol{E} = -\nabla V \tag{6}$$

where ρ_v, $\boldsymbol{D}$, V and $\boldsymbol{E}$ represent the charge density of the piezoelectric material, the potential shift vector, the electric potential and the resulting electric field vector, respectively. Figure 3d shows the piezoelectric potential and output power diagrams of the cantilever structure of the hybrid nanogenerator in the first-order and second-order bending characteristic frequency modes. The first-order and second-order resonance frequencies of the cantilever structure are 5.5 and 50 Hz, respectively, and the piezoelectric output performance in the second-order resonance mode is higher than that in the first-order resonance mode.

5 | DEMONSTRATION OF THE HP/TENG TO POWER WIRELESS SENSORS

The hybrid nanogenerator has the advantages of both TENG (low-frequency energy harvesting) and PENG (high output power), which are critical for powering electronic devices. The charging capability of the TENG, PENG and hybrid nanogenerator was verified by controlling the capacitor charging at 47 μF at a magnetic field strength of 4 Oe. Figure 4a shows that the HP/TENG obtained the highest charging voltage of the capacitor of 11 V within 10 s. It shows that the output performance and charging capability of the HP/TENG were much better than any of them. The charging capability of the HP/TENG was evaluated by varying the magnetic field strengths to 1, 2, 4, and 6 Oe. Figure 4b shows the charging voltage of 220 μF/25 V storage capacitor (Figure S5). It took 120 s for the capacitor to reach 3 and 6 V at 1 and 2 Oe AC magnetic field, respectively. As the applied magnetic field increased, the charging time naturally decreased. To demonstrate the capability of the hybrid nanogenerator in a self-powered sensing application, the cantilever beam system turns on commercial temperature and humidity sensors via the electrical energy storage and management circuit in the 2 Oe AC magnetic field generated using a Helmholtz coil. Figure 4c shows the principle of operation.

The output voltage of the hybrid MME generator is converted to a stable 3.6 V (Figure 4d) output voltage to power electronic devices via the energy storage and conversion circuit (LTC3588). When the sensor starts working, the sensor with an LCD screen and built-in bluetooth component can continuously display the ambient temperature and humidity and transmit the data to the cell phone receiver via bluetooth. These results demonstrate the viability of the hybrid MME generator cantilever as an energy source for self-powered systems, eliminating the magnetic energy prevalent around the power cables.

6 | CONCLUSION

In summary, we have demonstrated the HP/TENG for the stable/effective harvesting of electromagnetic energy to provide sustainable power for various commercial electronic devices. The device provided high output voltage/current and power of approximately 176 V/375 μA and 4.7 mW under 4 Oe magnetic field conditions. The HP/TENG produced a total power of approximately 2.08 times higher than that of the PENG and approximately 2.14 times higher than that of the TENG at optimal matching impedance. Combined with the appropriate energy management circuit, the device can continuously supply power to commercial temperature and humidity sensors. These results demonstrated the significant potential of the proposed magnetic field energy harvesting to enable specific self-powered sensor systems for smart buildings and industry.

ACKNOWLEDGEMENT

This work was supported by the State Grid Corporation of China through the Science and Technology Project under Grant 52094020006Z.

ORCID

Chaoyu Wang https://orcid.org/0000-0002-7862-2614
Yuchen Bai https://orcid.org/0000-0001-9963-9901

REFERENCES

1. Shrouf, F., Ordieres, J., Miragliotta, G.: Smart factories in industry 4.0: a review of the concept and of energy management approached in production based on the Internet of Things paradigm. In: IEEE international conference on industrial engineering and engineering management, Selangor, Malaysia, pp. 697–701 (2014)
2. Chung, M., Kim, J.: The internet information and technology research directions based on the fourth industrial revolution. KSII Trans. Internet Inf. Syst. 10(3), 1311–1320 (2016)
3. Minoli, D., Sohraby, K., Occhiogrosso, B.: IoT considerations, requirements, and architectures for smart buildings-energy optimization and next-generation building management systems. IEEE Internet Things J. 4(1), 269–283 (2017)
4. Yang, A., et al.: Single ultra thin WO_3 nanowire as a superior gas sensor for SO_2 and H_2S: selective adsorption and distinct IV response. Mater. Chem. Phys. 240, 122165 (2020)
5. Gui, Y., et al.: Platinum modified MoS 2 monolayer for adsorption and gas sensing of SF 6 decomposition products: a DFT study. High Volt. 5(4), 454–462 (2020)
6. Wang, X.H., et al.: Effects of adatom and gas molecule adsorption on the physical properties of tellurene: a first principles investigation. Phys. Chem. Chem. Phys. 20(6), 4058–4066 (2018)
7. Wang, D., et al.: Tellurene based chemical sensor. J. Mater. Chem. A. 7(46), 26326–26333 (2019)
8. Yang, A., et al.: Short period sinusoidal thermal modulation for quantitative identification of gas species. Nanoscale. 12(1), 220–229 (2020)
9. Chen, W., et al.: Review of optical fibre sensors for electrical equipment characteristic state parameters detection. High Volt. 4(4), 271–281 (2019)
10. Chu, J., et al.: Identification of gas mixtures via sensor array combining with neural networks. Sens. Actuators B Chem. 329, 129090 (2021)
11. Duan, L., et al.: Method of inter-turn fault detection for next-generation smart transformers based on deep learning algorithm. High Volt. 4(4), 282–291 (2019)
12. Al-Ali, A.R., et al.: A smart home energy management system using IoT and big data analytics approach. IEEE Trans. Consum. Electron. 63(4), 426–434 (2017)
13. Cheng, M., et al.: Overview of stator-permanent magnet brushless machines. IEEE Trans. Ind. Electron. 58(11), 5087–5101 (2011)
14. Wu, W., et al.: Lead zirconate titanate nanowire textile nanogenerator for wearable energy-harvesting and self-powered devices. ACS Nano. 6(7), 6231–6235 (2012)
15. Tadesse, Y., et al.: Multimodal energy harvesting system: piezoelectric and electromagnetic. J. Intell. Mater. Syst. Struct. 20(5), 625–632 (2009)

16. Wang, Z.L., Song, J.: Piezoelectric nanogenerators based on zinc oxide nanowire arrays. Science. 312(5771), 242–246 (2006)
17. Abdelmoula, H., et al.: Low-frequency zigzag energy harvesters operating in torsion-dominant mode. Appl. Energy. 204, 413–419 (2017)
18. Lu, Y., et al.: The PZT/Ni unimorphmagnetoelectric energy harvester for wireless sensing applications. Energ. Convers. Manag. 200, 112084 (2019)
19. Nan, C., et al.: Multiferroic magnetoelectric composites: historical perspective, status, and future directions. J. Appl. Phys. 103(3), 1 (2008)
20. Kambale, R.C., et al.: Magneto-mechano-electric (MME) energy harvesting properties of piezoelectric macro-fiber composite/Ni magneto-electric generator. Energy Harvest. Syst. 1(1-2), 3–11 (2014)
21. Xing, Z., Li, J., Viehland, D.: Giant magnetoelectric effect in Pb(Zr, Ti)O_3-bimorph/NdFeB laminate device. Appl. Phys. Lett. 93(1), 13505 (2008)
22. Liu, G., Ci, P., Dong, S.: Energy harvesting from ambient low-frequency magnetic field using magneto-mechano-electric composite cantilever. Appl. Phys. Lett. 104(3), 32908 (2014)
23. Kang, M.G., et al.: High power magnetic field energy harvesting through amplified magneto-mechanical vibration. Adv. Energy Mater. 8(16), 1703313 (2018)
24. Lee, H., et al.: Maximizing power generation from ambient stray magnetic fields around smart infrastructures enabling self-powered wireless devices. Energy Environ. Sci. 13(5), 1462–1472 (2020)
25. Cho, J.Y., et al.: Significant power enhancement method of magneto-piezoelectric energy harvester through directional optimization of magnetization for autonomous IIoT platform. Appl. Energ. 254, 113710 (2019)
26. Huang, L.B., et al.: Magnetic-assisted noncontact triboelectric nanogenerator converting mechanical energy into electricity and light emissions. Adv. Mater. 28(14), 2744–2751 (2016)
27. Lim, K.W., et al.: A high output magneto-mechano-triboelectric generator enabled by accelerated water-soluble nano-bullets for powering a wireless indoor positioning system. Energy Environ. Sci. 12(2), 666–674 (2019)
28. Shi, Y., et al.: A novel self-powered wireless temperature sensor based on thermoelectric generators. Energy Convers. Manag. 80, 110–116 (2014)
29. Iqbal, M., Khan, F.U.: Hybrid vibration and wind energy harvesting using combined piezoelectric and electromagnetic conversion for bridge health monitoring applications. Energy Convers. Manag. 172, 611–618 (2018)
30. Zhao, D., Han, N.: Optimizing overall energy harvesting performances of miniature Savonius-like wind harvesters. Energy Convers. Manag. 178, 311–321 (2018)
31. Kang, M., et al.: Recent progress on PZT based piezoelectric energy harvesting technologies, pp. 5. Multidisciplinary Digital Publishing Institute (2016)
32. Xing, Z., et al.: Giant magnetoelectric torque effect and multicoupling in two phases ferromagnetic/piezoelectric system. J. Appl. Phys. 110(10), 104510 (2011)
33. Niu, S., et al.: Theoretical study of contact-mode triboelectric nanogenerators as an effective power source. Energy Environ. Sci. 6(12), 3576–3583 (2013)
34. Zou, H., et al.: Quantifying and understanding the triboelectric series of inorganic non-metallic materials. Nat. Commun. 11(1), 1–7 (2020)
35. Shi, K., et al.: Dielectric modulated cellulose paper/PDMS-based triboelectric nanogenerators for wireless transmission and electropolymerization applications. Adv. Funct. Mater. 30(4), 1904536 (2020)
36. Zou, H., et al.: Quantifying the triboelectric series. Nat. Commun. 10(1), 1–9 (2019)

SUPPORTING INFORMATION

Additional supporting information may be found online in the Supporting Information section at the end of this article.

How to cite this article: Yang, A., et al.: Hybrid piezo/triboelectric nanogenerator for stray magnetic energy harvesting and self-powered sensing applications. High Volt. 6(6), 978–985 (2021). https://doi.org/10.1049/hve2.12096